An X-ray Absorption Near Edge Structure Spectroscopy Study of Metal Coordination in Co(II)-Substituted *Carcinus maenas* Hemocyanin

S. Della Longa,* A. Bianconi,* L. Palladino,* B. Simonelli,‡ A. Congiu Castellano,‡ E. Borghi,§ M. Barteri,§ M. Beltramini,¶ G. P. Rocco,¶ B. Salvato,¶ L. Bubacco,‖ R. S. Magliozzo,‖ and J. Peisach‖

*Dipartimento Medicina Sperimentale, Università dell'Aquila, 67100 L'Aquila, Italy; ‡Dipartimento Fisica and §Dipartimento Chimica, Università di Roma "La Sapienza," 00185 Rome, Italy; ¶Dipartimento Biologia, Università di Padova, 35121 Padova, Italy; and ‖Albert Einstein College of Medicine, Yeshiva University, Bronx, New York 10461 USA

ABSTRACT High-resolution x-ray absorption near edge structure spectroscopy was used to characterize the metal sites in three different cobalt-substituted derivatives of *Carcinus maenas* hemocyanin (Hc), including a mononuclear cobalt, a dinuclear cobalt and a copper-cobalt hybrid derivative. Co(II) model complexes with structures exemplifying octahedral, trigonal bipyramidal, pseudo-tetrahedral, and square planar geometries were also studied. The results provide structural information about the metal binding site(s) in the Co-Hcs that extend earlier results from EPR and optical spectroscopy (Bubacco et al. 1992. *Biochemistry.* 31:9294–9303). Experimental spectra were compared to those calculated for atomic clusters of idealized geometry, generated using a multiple scattering approach. The energy of the dipole forbidden 1s→3d transition and of the absorption edge in the spectra for all cobalt Hc derivatives confirmed the cobaltous oxidation state which rules out the presence of an oxygenated site. Comparisons between data and simulations showed that the mononuclear and dinuclear Co(II) derivatives, as well as the hybrid derivative, contain four-coordinate Co(II) in distorted tetrahedral sites. Although the spectra for Co(II) in dinuclear metal sites more closely resemble the simulated spectrum for a tetrahedral complex than do spectra for the mononuclear derivative, the Co(II) sites in all derivatives are very similar. The Cu K-edge high resolution x-ray absorption near edge structure spectrum of the hybrid Cu-Co-Hc resembles that of deoxy-Hc demonstrating the presence of three-coordinate Cu(I).

INTRODUCTION

Hemocyanin (Hc) is an oxygen transport protein found in the hemolymph of several species of *Mollusca* and *Arthropoda* (Ellerton et al., 1983; Salvato and Beltramini, 1990). The structure of *Panulirus interruptus* Hc (*Arthropoda)* has been solved to 3.2 Å resolution by x-ray diffraction (Gaykema et al., 1984; Linzen et al., 1985; Volbeda and Hol, 1986), and a refinement of the 3.2-Å resolution data was reported (Volbeda and Hol, 1989). More recently, the structure of subunit II of *Limulus polyphemus* oxy-Hc was solved to 2.2-Å resolution (Magnus and Ton-That, 1992). In this case, each five-coordinate, square-pyramidal Cu ion is shown to be bound to the protein by three histidyl imidazole nitrogen atoms and to a dioxygen molecule. The copper-copper distance in this site is approximately 3.5 Å. In the deoxy- form, the coordination number is reduced to three and each cuprous copper is bound to two imidazole nitrogens at 1.9 Å, and to a third imidazole nitrogen at 2.7 Å. The coordination symmetry of the three imidazoles to each Cu atom is approximately C_{3v} around the Cu-Cu axis (Gaikema et al., 1984).

A variety of chemical and spectroscopic studies have been undertaken to probe the structure of the dinuclear metal center. Electron paramagnetic resonance (EPR) and optical spectroscopy, although potentially useful for studying metal sites, cannot probe the structure of deoxy-Hc, because the two Cu(I) ions are EPR silent and exhibit uninformative ultraviolet-visible spectra. Although oxy-Hc exhibits some properties of a cupric ion, it also is EPR silent because of antiferromagnetic coupling mediated by the bound dioxygen molecule (Solomon et al., 1976; Dooley et al., 1978).

Information about ligand type, coordination number, and bond lengths has also come from copper extended x-ray absorption fine structure (EXAFS) spectroscopy of oxy- and deoxy-Hc from a variety of species (Woolery et al., 1984; Brown et al., 1980; Co et al., 1981; Feiters, 1990; Blackburn et al., 1989). X-ray absorption near edge spectroscopy (XANES), a related technique, provides information unavailable from EXAFS concerning the geometry and valence state of metal ions. XANES can be usefully applied to the study of native and metal-substituted hemocyanins (Brown et al., 1980) and can probe differences in geometry between sites having equivalent coordination number. Cu x-ray absorption edge spectra for a large series of Cu(I) and Cu(II) complexes, including the multi-copper oxidase laccase, have also been reported (Kau et al., 1987).

In the present study, the XANES technique was used to characterize the metal sites of native Cu-containing oxy- and deoxy- forms of *Carcinus maenas* Hc and its Co-substituted derivatives. These included a mononuclear (Salvato et al., 1986) and dinuclear cobalt species and a hybrid that contains one Cu and one Co in the active site (Bubacco et al., 1992). Also examined were several Co(II) model complexes. An aim in this report is to characterize the metal binding site of the cobalt-substituted derivatives and to determine the valence state of the cobalt in the dinuclear derivative, since the EPR spectrum of the latter does not exhibit the signal intensity expected for two independent Co(II) ions, suggesting either spin coupling or oxidation to Co(III) (Bubacco et al.,

Received for publication 2 March 1993 and in final form 7 September 1993.

Address reprint requests to Dr. S. Della Longa, Dipartimento Medicina Sperimentale, Università dell'Aquila, via S. Sisto 20, 67100 L'Aquila, Italy.

0006-3495/93/12/2680/12 $2.00

1992). Also, the EPR signal of the monocobalt derivative, although characteristic of high-spin Co(II), does not provide unambiguous information concerning the coordination number of the metal ion. Finally, the issue of oxygen binding by the dinuclear $Co(II)_2$-Hc is addressed through the elucidation of the oxidation state of the metal ions. Although other reports published on cobalt-substituted Hc have suggested a tetrahedral site for the bound metal ion (Suzuki et al., 1982; Loroesch and Haase, 1986; Dutton et al., 1990), the presence of unspecifically bound metal compromised a structural characterization of cobalt bound only at the active site.

Simulation of spectra using a multiple scattering (MS) scheme provides a structural analysis of the XANES spectra and of the small but significant changes in the series of spectra for the various derivatives. The results provide a clear demonstration of the coordination number, geometry, and oxidation state of the metal ions in the Co-containing Hc derivatives .

EXPERIMENTAL PROCEDURES

Materials

C. maenas Hc was purified as described by Salvato et al., 1986. A mononuclear derivative containing a single Co(II) at the active site Co(II)-Hc, and a dinuclear derivative, $Co(II)_2$-Hc, were prepared from the apoprotein; the hybrid derivative, Cu(I)-Co(II)-Hc, was prepared from native Hc (Bubacco et al., 1992). Although the chloride and thiocyanate present in the reconstitution mixture might be tightly bound in the cobalt derivatives, their presence is ruled out based on the EXAFS analysis of these derivatives (L. Bubacco, R. S. Magliozzo, L. Powers, and J. Peisach, unpublished observations). Some Hc samples used for XANES spectroscopy were prepared by lyophilization of protein solutions in phosphate buffer to which 1:2 w/w sucrose was added. Other samples were examined in glycerol solution. These were prepared by ultracentrifugation of the aqueous protein solution containing 150–200 mg of Hc (with a Beckman XL70 ultracentrifuge and a 70Ti rotor) at 60,000 rpm (371,000 × g) for 4 h. The pelleted protein was redissolved in 1 ml of 5 mM Tris-HCl buffer at pH 7.0 containing 50% w/w glycerol and was stored at −20°C until used.

The model compound $[Co(Et_4dien)Cl_2]$, with Et_4dien = bis(2-diethylaminoethyl)amine, prepared as described elsewhere (Ciampolini and Speroni, 1966). The Co structure is approximately trigonal bipyramidal with a chlorine and a nitrogen in the apical positions (Dori et al., 1967). The ligand *N*-(*o*-hydroxy-benzylidene)ferroceneamine = L, a Schiff base molecule carrying a ferrocenyl group, and its metalated complex, $Co(II)L_2$, were prepared as previously described (Bracci et al., 1990). An x-ray diffraction analysis (Bracci et al., 1990) of the copper analogue, $Cu(II)L_2$, shows a distorted tetrahedral geometry for this complex. On the basis of visible spectra and magnetic susceptibility data (Bracci et al., 1990), the $Co(II)L_2$ complex contains high-spin Co(II) and is used here as an example of a pseudo-tetrahedral structure. Phthalocyaninatocobalt (II), Co(PC), was purchased from Eastman, and was purified by vacuum sublimation (10^{-2}-10^{-3} Torr) at 400–450°C. A square planar geometry for the four-coordinate low-spin Co(II) has been reported for this compound (Kasuga and Tsutsui, 1980; Moser and Thomas, 1983).

X-ray absorption spectra for Co and Cu were collected up to 120 eV above the K-edge using the Wiggler beam line of the Adone storage ring at the Laboratori Nazionali of Frascati. Transmission mode was used for the lyophilized or powder samples and fluorescence mode for samples in solution. Spectra were acquired with an average current of 30 mA at 1.5 GeV electron energy. High resolution (0.5 eV) was achieved using a Si (111) monochromator with a 1-mm entrance slit. The signal-to-noise ratio was usually 20 at the absorption edge. The acquisition of fluorescence data was performed using two NaI(Tl) Teledyne scintillation detectors positioned at 90° with respect to the beam. The samples, positioned at 45°, were contained in Teflon cells with 2-mm thick Mylar windows. Spectra were recorded at room temperature. A straight line fitting the background was subtracted from the data and the final form of the curves was plotted after application of a smoothing function. In all experimental spectra presented here, the energy 0 is fixed at the absorption threshold for metallic reference foils.

Methods

The XANES signal

In the one-electron approximation, the absorption coefficient $\mu(E)$ is determined by dipole transitions from the core level, c, characterized by the quantum numbers n and ℓ with energy E_c, to the jth unoccupied state with energy E_j. An electron from a core level having angular momentum ℓ is excited into the $\ell \pm 1$ final state. In a K-edge spectrum, only the $\ell = 1$ (p-like) final states are allowed by the $\Delta\ell = +1$ dipole selection rule. Modulations of the x-ray absorption signal above the absorption threshold in the XANES (0–60 eV) and EXAFS (60–1000 eV) regions are interpreted as continuum resonances due to the interference between the photo-emitted and the scattered electron waves within the atomic cluster surrounding the metal (Durham, 1988). In the MS approach in real space, the total absorption coefficient $\mu(E, \epsilon)$ (with energy E and polarization vector ϵ) can be expressed as

$$\mu(E, \epsilon) = \mu_0(E)\,[1 + \sum_{2}^{\infty}{}_n \chi_n(E, \epsilon)],$$

in which $\chi_n(E, \epsilon)$ are the modulations of the atomic absorption coefficient $\mu_0(E)$, due to the scattering pathways of the emitted photoelectron starting and ending at the central atom involving $n-1$ neighboring atoms. The first term of the sum, $\chi_2(E, \epsilon)$ represents single scattering contributions, i.e., the EXAFS signal. The shape and the intensity of the multiple scattering resonances depend on scattering pathways that give non-negligible contributions to the interference process, hence they depend on the geometry and size of the cluster and on the type of ligand.

XANES simulation: construction of the molecular potential

The MS calculation is done in the frame of the one-electron theory by using a non-self-consistent molecular electron potential. The scattering properties of the surrounding atoms on the photoelectron generated by core excitation are described by the atomic phase shifts experienced by the photoelectron wave when it encounters each surrounding atom, i.e., its potential in the "muffin tin" (MT) form (Pendry, 1974). The MT potential is calculated around each atomic species (the MT spheres) by first superimposing and spherically averaging the shells of atomic charge densities around the central atom, then solving the Poisson equation for the Coulombic part of the potential. An exchange-correlation potential is added using a local approximation of the X_α type (Slater, 1979; Kutzler et al., 1980; Doniach et al., 1984), where α is the Slater exchange factor. The MT description of the potential is routinely used in the calculation of energy bands in solids, and has been successfully applied to calculate XANES spectra of high symmetry molecular systems, but it is expected to be less accurate for low symmetry clusters. Notwithstanding these limitations, the MT approximation has been found to be rather accurate for a variety of species, including extended asymmetric metallic sites in proteins (Bianconi et al., 1985) and ionic materials (Kitamura et al., 1987).

After core excitation, the electrons in the excited atom experience a different potential due to the excited electron-hole dipole. Since the nucleus is less screened after removing the core electron, the wave functions of the passive electrons are pulled in toward the nucleus by attractive interaction with the core and relax to lower energy. Therefore, the description of this scattering process is a (time-dependent) many-body problem. However, the need to consider the time dependent relaxation can be removed assuming that the potential seen by the photoelectron is the static potential that exists after all passive electrons are fully relaxed. In this way the description of the scattering process is reduced to a one-electron problem. Therefore, phase shifts and scattering amplitudes can be calculated using this fully relaxed potential. In the $Z + 1$ approximation, the fully relaxed MT potential around the central atom is closely approximated by that of an atom with an atomic

number greater by one unit (Bianconi et al., 1988). Hence in the following, when we refer to the scattering properties of the absorbing Co (i.e., MT radius and phase shifts) that of Ni are to be intended.

Our criterion of choosing the radii of the MT spheres is as follows: as a first step, we compute the MT potential choosing non-overlapping MT radii (R_{MT}) of each atomic species (i.e., Co, N, O, and C) as the radii at which the neutral atomic potentials of neighboring atoms intersect. The values determined for the first pair of neighbors are extended to all the other shells. After this first step one obtains different values V_{MTi} of the MT potential at the boundary of each MT sphere (where i indicates the atomic species). The MT radii are then refined, under the limits of non overlapping spheres, by searching for the minimal deviation of these different values from their averaged value V_{MT}. The value V_{MT} is taken as the interstitial constant of the MT potential. In the case of very simple (ordered) systems, such as monatomic or diatomic crystals with cubic symmetry, MT radii corresponding to a convergence of V_{MTi} values within 0.01 eV are determined automatically by a computer program, using a multivariable minimization algorithm. However, in the case of the Co(II) clusters relevant to the Hc active site structure, with very low symmetry and four atomic species, we found an unsatisfactory discontinuity of the interstitial potential. We then found a very low discontinuity using only two atomic species, Co and N (i.e., obtaining phase shifts of N for O, N, and C atoms). This approximation is justified by assuming that the scattering parameters for the element of atomic number Z and its $Z - 1$ and $Z + 1$ neighbors are similar. The final choice was R_{MT}(Co) = 1.09 Å and R_{MT}(N) = 1.05 Å. The validity of the choice of the MT radii is then tested by the reproduction of the XANES spectra of known structures (see Fig. 2). Although the final choice can be poorly related to other molecular properties, it is the best way to reduce the discontinuities of the potential and to make the calculations meaningful. The value of the intersphere constant was $V_{MT} = -19.76$ eV with a discontinuity of less than 0.04 eV. This value is found below the continuum threshold (also called vacuum level), so in the XANES simulation, two energy regions will be differentiated: 1) the region from the V_{MT} value to the vacuum level, containing localized, quasi-atomic electron states; and 2) the region beyond the vacuum level, containing highly delocalized molecular electronic states.

XANES simulation: multiple scattering calculations

The calculations in real space using the full multiple scattering formalism were carried out using our G4XANES procedure, assembled by merging and extending several pre-existing programs. This unique procedure, described elsewhere (Li et al., 1991; Palladino et al., 1993) has been used to perform XANES simulations on different kinds of compounds, e.g., crystals (Li et al., 1991), small molecules (Palladino et al., 1993), and low-symmetry metal sites in proteins (Amiconi et al., 1989; Congiu Castellano et al., 1991, Della Longa et al., 1992), and minimizes the arbitrary choices in the construction of the MT potential. The input for the calculations are the appropriate atoms and the coordinates of the metal cluster. In the case of simple (ordered) systems, such as monoatomic or diatomic crystals with cubic symmetry, true ab initio calculations are performed, because no other input data are required. In fact, the MT radii are automatically found by the program, as described above, and the other unknown parameters, as the Slater exchange factor, are fixed in the program at their default values (Li et al., 1991). The procedure then calculates the MT potential and the atomic phase shifts and the output is the XANES spectrum.

The final program of the procedure (an extension of that of Durham et al., 1982) calculates the angular momentum selected transition probabilities to occupied and unoccupied electronic states beyond V_{MT}. To simulate K-edge XANES spectra, we calculate the transition probabilities starting from the deep metal core level 1s ($\ell = 0$, $m_\ell = 0$) to delocalized final states with p-symmetry ($\ell = 1$, $m_\ell = 0,1$). Therefore the program calculates $E//z$ ($m_\ell = 0$) and $E//xy$ ($m_\ell = 1$) polarized XANES spectra. The unpolarized spectrum is obtained by a 2:1 weighted sum of the $E//xy$ and $E//z$ spectra. The program can work without any limitation in symmetry. Symmetry parameters are handled by the program, however, by assuming that the cluster has a rotational axis of symmetry and/or a mirror plane. Scattering that depend on z-oriented pathways are distinguished from those of planar xy-oriented pathways by the polarized calculations. Thus, the contributions of axial and equatorial scattering may be treated separately and the changes in the unpolarized spectrum can be interpreted in terms of structural changes in the atomic cluster.

A key factor in the XANES calculations using the MS procedure is the size of the cluster, i.e., the number of scattering shells considered. The size is determined by the electron inelastic mean free path and the core-hole lifetime, and is usually the same as that probed by EXAFS. For highly ordered systems (i.e., crystals), clusters up to 7 Å are known to contribute to the observed spectrum (Bianconi, 1988). For samples with high structural disorder, such as solutions and amorphous compounds, often just a single shell analysis can reproduce the most prominent spectroscopic features. Calculation of the polarized spectra for increasing cluster size, i.e., including additional atomic shells, enables the extraction of additional information relevant to the structure of ligands.

Comparison between theory and experiment: broadening factors

To compare calculated spectra with XANES data collected for dilute samples, a broadening function may be required to convolve the numerical results of the MS calculation. The width of the broadening function depends on many factors, some of which are energy-dependent, and only a few are known a priori for the compound studied. We have convolved our data with a Lorentzian function with a Γ factor resulting from summing an experimental resolution of 0.5 eV, a lifetime broadening of 1.3 eV (Krause and Oliver, 1979), and an energy dependent factor representing the photoelectron lifetime due to the inelastic scattering with valence electrons. This energy-dependent term has been extracted starting from the integral of the measured electron energy loss function in different Cu compounds (Fink et al., 1989), in the range from 0 to 40 eV. This procedure gives an estimate of the total energy dependent broadening factor, but its actual values are adjusted by comparison with the experimental spectra.

Finally, the energy alignment of the calculated spectrum to the experimental one is done by superimposing the $1s \rightarrow 3d$ calculated transition with the experimental pre-edge peak P in the derivative spectrum.

Discussion of errors in XANES simulations

The limitations and errors in the XANES simulation for biological compounds arise from different factors. First, the basic approximations of the procedure (use of a non-self-consistent potential generated by a model cluster) involves systematic errors that depend on the model chosen. For example, in calculating the MS XANES for the octahedral single-shell Co-N_6 cluster, a different choice of the molecular potential in the MT approximation, obtained by changing the atomic MT radii by about 10% and leaving the same Co-N distance, induces spectral changes equivalent to a 0.01–0.03 Å variation of the Co-N distance in the model without a change in MT radii. Poorer approximations resulting in larger errors will pertain as the asymmetry of the first shell increases. The second factor involves the uncertainty due to the atomic Debye-Waller factors that account for structural and thermal disorder. Last, the presence of more than one molecular structure, i.e., different conformational substates at the metal site, as shown for the Fe site in myoglobin (Hong et al., 1990), cannot be excluded, whereby the experimental spectrum will be due to a weighted sum of the populations of each molecular configuration at a given temperature. A XANES computation including molecular dynamics, however, is beyond the scope of the present work.

The overall systematic errors are therefore in practice much larger than those implicit in the relatively high sensitivity of the MS XANES calculations to simulated structural changes of an ideal compound (in the example of the Co-N distance in octahedral CoN_6 cluster it is less than 0.01 Å).

For known structures, a very good agreement is found between calculations and experimental XANES spectra in terms of the energies of the peaks, although a poorer agreement for their intensity is expected. Although these limitations must be considered when attempting to derive information about the interatomic distances and geometry, it is clear from the results presented below that the structural origin of changes in spectral features can be analyzed and understood.

RESULTS

Co(II) model compounds

Fig. 1 shows the spectra of hydrated $CoSO_4$, Co(II)(Et_4dien)-Cl_2, Co(II)L_2, and CoPC. Crystalline $CoSO_4$ is orthorhombic with four molecules per unit cell, and the coordination around Co(II) is a distorted octahedron (Wyckoff, 1964) with an average Co-O distance of 2.1 Å. The K-edge XANES spectrum of $CoSO_4$ shows a sharp main peak above the absorption threshold, at approximately 16 eV (Fig. 1 *C*). The intensity ratio between this peak and the atomic absorption jump is 1.5. This high ratio and the sharpness of the peak is typical of octahedral Co(II) complexes. The MS theory shows that this peak receives resonant, in-phase contributions from both single scattering and successive orders of collinear multiple scattering pathways (Bianconi et al., 1988). The pre-edge region (from −5 to 5 eV) and the rising edge region (from 5 to 12 eV), are devoid of relevant features, whereas a multiple scattering broad peak arises at about 29 eV (Fig. 1 *D*).

The complex Co(II)(Et_4dien)Cl_2, whose spectrum is shown as the second curve in Fig. 1, is five-coordinate with three nitrogen and two chlorine ligand atoms, according to the x-ray structure (Dori et al., 1967; Di Vaira and Orioli, 1969). The geometry of this complex is close to trigonal bipyramidal with one Cl at 2.32 Å and one N at 2.16 Å in the axial positions. The bond lengths for the two other nitrogen atoms are 2.19 and 2.21 Å. The bond length for the second Cl is 2.36 Å. The XANES spectrum of this compound shows a shoulder on the rising edge at 8 eV (*B*) and shows features near 12, 17 and 29 eV. A weak pre-edge peak (*P*) at 1 eV is present. The intensity ratio between the main peak and the atomic absorption jump is 1.2, somewhat lower than that for the six-coordinate species above. The lower intensity ratio in four-coordinated and five-coordinated species is according to MS theory attributed to a lower number of collinear multiple scattering pathways with respect to octahedral complexes. In particular, the tetrahedral cluster has the characteristic that there are no MS pathways with atoms in collinear positions.

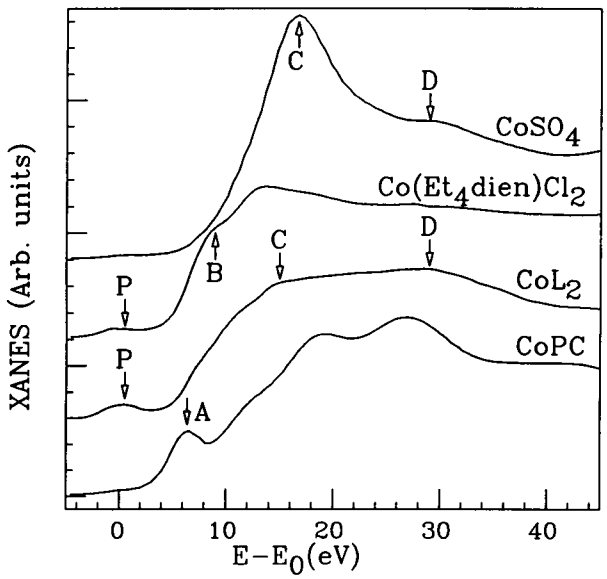

FIGURE 1 K-edge XANES spectra of Co(II) compounds. From *top* to *bottom:* octahedral Co(II)SO_4, five-coordinate Co(II)(Et_4dien)Cl_2, four-coordinate tetrahedral Co(II)L_2, and four-coordinate square-planar Co(II)-phthalocyanine.

The third curve in Fig. 1 shows the XANES spectrum of Co(II)L_2. The x-ray structure of this complex has not been solved, but x-ray crystallography of the analogous Cu(II) complex shows a flattened tetrahedral coordination (Bracci et al., 1990) with copper-nitrogen bond lengths of 1.95 and 1.99 Å, and copper-oxygen bond lengths of 1.88 and 1.90 Å. The Co(II)L_2 complex is reported to be pseudo-tetrahedral according to visible and near infrared absorption spectra (Lever, 1984). New features for this complex include an increase of the intensity of the pre-edge peak at 1 eV and a general broadening and decrease of the intensity of the sharp main peak at 16 eV (*C*) concomitant with an increase of the intensity of the feature at 29 eV (*D*). The 1 eV pre-edge peak (*P*) is generally assigned to a dipole allowed transition from the 1s to an unoccupied anti-bonding orbital t_2 for tetrahedral transition metal clusters of the type MO_4 (Kutzler et al., 1980; Bianconi, 1988). The final state has d orbital symmetry and its intensity depends on the valence of the metal; it is negligible for absorbing metals with filled d shells, e.g., Cu(I) ($3d^{10}$) and it is very strong for V(III) ($3d^0$). For the same metal in different environments, the intensity of 1s → 3d transition depends on the coordination geometry. It is completely dipole-forbidden for centro-symmetric octahedral symmetry, but has non-zero intensity for non centro-symmetric clusters, and it has strong intensity for tetrahedral clusters due to the metal d-p orbital mixing through the perturbation of the ligand field. Other mechanisms are known to give minor contributions to the intensity of the pre-edge peak, such as the allowed magnetic dipole and electric quadrupole transitions, metal 3d-ligand orbital mixing, and vibronic coupling with the metal-ligand bond vibrations (Sano et al., 1992).

The bottom curve of Fig. 1 shows the XANES spectrum of the square planar complex, CoPC. Transition metal complexes with D_{4h}, D_{2d}, and D_{2h} symmetry exhibit a characteristic shoulder at the absorption edge (peak *A* at ~6 eV) the origin of which is still debated. In recent years, most discussions have focused on its origin in Cu(II) square planar compounds and many electron processes considered by a self-consistent-field approach have been invoked. The shoulder has been interpreted as a 1s → 4p transition simultaneous with a ligand-to-metal shakedown (Kosugi et al., 1984). Alternatively, one electron MS calculations have successfully reproduced the XANES spectra of tetragonally distorted metal complexes (Palladino et al., 1992). The shoulder, in the MS scheme, arises from a 1s → εp quasi-bound resonance, polarized perpendicular to the coordination plane.

The general shapes and features of the spectra in Fig. 1

are reproduced by the calculated XANES spectra shown in Fig. 2. Calculated spectra for single shell clusters are shown, including those for octahedral CoN_6, trigonal bipyramidal CoN_5, tetrahedral CoN_4, and tetragonally distorted (square planar) CoN_4N_2.The Co-N distances were set equal to 2.0 Å in all cases except for the axial Co-N distances in the model CoN_4N_2, which were set to 2.7 Å. It is noteworthy that the spectra of Fig. 1 are satisfactorily reproduced by the calculated spectra of Fig. 2, in spite of the rough approximation of the actual bond distances, angles, and atomic species used (N vs. Cl ligands), showing that the idealized symmetry of the first shell is sufficient in many cases to determine the shape of the XANES spectrum. For clusters with O_h symmetry (CoN_6) or T_d symmetry (CoN_4) no polarization effect occurs. When a *z*-tetragonal distortion is present, an energy splitting of the *E//z* polarized absorption maximum from the *E//xy* polarized absorption maximum is calculated, giving rise to the $1s \rightarrow \epsilon p$ shoulder (due to the *E//z* component) in the unpolarized spectrum, whose magnitude and position depends on the degree of the distortion. This XANES dichroism explains the shape of the absorption threshold in CoPC.

It is worth noting that when d-p mixing occurs (for example in CoN_5 with C_{3v} symmetry or in CoN_4 with T_d symmetry), the 3d perturbed states of the metal develop p-character, and give peaks or bands in the low energy region of MS calculated K-XANES spectra. This is the origin of the *P* peak in the simulations for CoN_4 and CoN_5 clusters. Since the simulation programs calculate the transition probability to occupied and unoccupied final states, the peaks calculated for the 3d perturbed energy levels may be totally or partially occupied depending on the valence state of the metal.

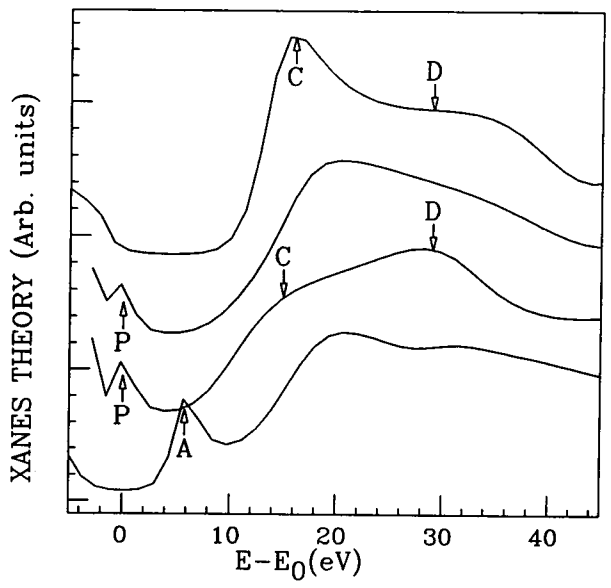

FIGURE 2 Calculated Co K-edge XANES spectra of simple clusters. From *top* to *bottom:* octahedral CoN_6, trigonal bipyramidal CoN_5, tetrahedral CoN_4, tetragonal (square planar) CoN_4N_2. All Co-N distances are equal to 2.0 Å except for the axial Co-N distance in tetragonal CoN_4N_2, which is set to 2.7 Å.

XANES spectra for Co(II)-substituted *C. maenas* hemocyanin

The Co K-edge XANES spectra of three Co-substituted *C. maenas* Hc derivatives are shown in Fig. 3 *A*: the dinuclear $Co(II)_2$-Hc derivative in sucrose solution (*bottom curve*), the lyophilized dinuclear $Co(II)_2$-Hc derivative (*middle curve*), and the lyophilized mononuclear Co(II)-Hc derivative (*top curve*). The energies of spectral features *P, B, C,* and *D* are given in Table 1. In Fig. 3 *B* the first derivatives of the spectra in Fig. 3 *A* are shown in the same order revealing the energies of the spectral features β, γ, and δ which are given in Table 1. Fig. 3 *C* shows the second derivatives (multiplied by −1) of the spectra, which are useful in evaluating the energy of the features *B, C,* and *D*.

The spectrum of the dinuclear derivative in solution is the same as that of the lyophilized sample and show broadened threshold features and the pre-edge peak, *P*, at 1 eV. The similarity demonstrates that the lyophilization process does not alter the structure of the $Co(II)_2$-Hc metal binding site. The energy of the pre-edge peak and of the absorption threshold for the dinuclear and the mononuclear derivatives are the same as those of the model $Co(II)L_2$. Therefore, the oxidation state of cobalt in the Hc derivatives is demonstrated to be 2+, in accord with evidence from EPR for the mononuclear derivative and optical spectra for both mononuclear and binuclear forms (Bubacco et al., 1992). The presence of Co(III) is ruled out since the energy threshold would be 2–3 eV higher for the cobaltic ion in the same symmetry, following the energy shift of the 1s core level binding energy due to the variation of the metal charge (Bianconi, 1988). The intensity of the well defined pre-edge peak and the low intensity ratio (1.25) between the main peaks, *C* and *D*, and the absorption jump indicate that the Co sites in both the mono and dinuclear Hc derivatives are four-coordinate, with geometries close to tetrahedral (Yachandra et al., 1983). The results also demonstrate that both Co(II) ions in the dinuclear derivative are bound in similar sites, suggesting that the active site is fully loaded.

A comparison of the first derivative spectra for the mono- and dinuclear cobalt derivatives indicates that all features occur at the same energy for both species. Therefore, any differences between the structure of the mono- and dinuclear cobalt binding sites can be explained by changes in bond angles and not in bond lengths (Bianconi et al., 1988). The pre-edge peak is larger for the dinuclear cobalt Hc, suggesting that the geometry of Co(II) is closer to tetrahedral when two metal ions are present in the active site. A weak feature (*B*) is present in all spectra. The single-shell calculation does not predict this feature and it is necessary to include three shells to reproduce it (see below). The feature *A* (Fig. 2, *bottom*), typical of square plane complexes, is absent. Finally, we note that the three curves have different intensity

TABLE 1 Energy position of the features in Co K-edge spectra (± 0.5 eV)

Samples	*P*	*B*	*C*	D	β	γ	δ
$Co(II)_2$-Hc*	1.0	12.0	18.0	25.0	11.0	15.5	23.0
$Co(II)_2$-Hc‡	1.0	11.5	18.0	23.5	10.5	15.5	21.0
Co(II)-Hc‡	1.0	11.0	17.0	23.0	10.0	15.0	19.0
Cu-Co-Hc*	1.0	14.0	18.0	22.5	10.5	12.0	16.5

* Compound in sucrose solution.
‡ Lyophilized sample.

ratios, *C/D,* indicating a different long-range order around the Co site (see below).

MS simulations of Co(II) clusters relevant to the Hc active site structure

The single-shell calculation for the tetrahedral CoN_4 cluster shown in Fig. 2 does not reproduce all the features that appear in the spectra of Co(II)-Hcs. To improve our analysis, we have calculated the polarized XANES spectra for additional model clusters. In Fig. 4 we show the single shell MS calculation for a hypothetical three-coordinate C_{3v} cluster, $Co(N)_3$ related to the structure of deoxy-Hc and the three-shell simulation for a $Co(imid)_3$ cluster including a second cobalt ion at 3.6 Å. The first shell in these models has three nitrogen ligand atoms at a distance of 1.95 Å. The displacement of the Co from the plane defined by the three nitrogen atoms is 0.6 Å. In the $Co(imid)_3$ model, the three imidazole rings are oriented with their planes parallel to the C_3 axis, and this axis is chosen as the *z*-direction in our calculations. The second shell contains six carbon atoms and the third shell contains three carbon atoms, three nitrogen atoms, and one cobalt atom, leading to the notation $Co\text{-}(imid)_3\text{-}Co$.

We have carried out three-shell calculations both in the presence and in the absence (not shown) of a second Co atom, at a distance of 3.6 Å from the central one, on the *z* axis. The results for these simulations show that the effect of a second Co atom on the calculated spectrum is so weak that its contribution must be negligible in the experimental one. This is very different from the behavior observed in EXAFS results. For example, in the Cu K-edge of hemocyanin, a well-defined single peak in the Fourier transform of the EXAFS signal has been assigned to a Cu-Cu single scattering resonance (Brown et al., 1980). An explanation is found by examining the scattering parameters of the atoms. The backscattering amplitude $F(k)$ and phase $\phi(k)$ (k is the photoelectron wave number) are energy-dependent. For example, treating the photoelectron wave as a plane wave (Teo and Lee, 1979), the calculated $F(k)$ for Cu is about 0.7 Å for $k \approx 7$ Å^{-1} (in the EXAFS region) but becomes low, $F(k)$ 0.35 Å for $k \approx 3$ Å^{-1}, in the XANES region. In contrast, the multiple scattering signal coming from imidazole rings is weak at high energy, but becomes strong for lower energies of the photoelectron, in the XANES region. So the Co-Co single scattering signal, probably relevant in EXAFS, is completely suppressed in XANES by the strong multiple scattering of the imidazole rings. Hence, in comparing the Co K-edges of Co(II)-Hc, Cu(I)-Co(II)-Hc, and $Co(II)_2$-Hc derivatives, the differences in the XANES spectra are expected to result from changes in ligand geometry around Co, without any direct contributions from Cu-Co or Co-Co single scattering effects.

The calculated single-shell spectra for the three-coordinate $Co(N)_3$ cluster (Fig. 4, *bottom*) show the feature P below the vacuum level due to the 1s→3d transition (*E//xy* polarized, 8 eV above V_{MT}), and the broad band *A* arising from localized p-states (*E//z* polarized). The band *A* has the same origin here as in tetragonally distorted metal complexes discussed above and gives rise to a shoulder at the absorption threshold in the unpolarized spectrum. The *E//xy* polarized spectrum has the same shape as that shown for the tetrahedral cluster in Fig. 2, as expected due to the similarity between T_d and C_{3v} symmetry clusters. The single-shell calculation gives no resolved features in the continuum energy region and is therefore inadequate to simulate the experimental spectra.

In the three-shell calculation of Fig. 4, in addition to a weak perturbation of the peak *P* and the band *A*, the new features, *B* and *C* appear at 22 and 27 eV above V_{MT}. The peak *D*, at 34 eV above V_{MT}, represents contributions from the first shell (three imidazole nitrogens) and multiple scattering from further shells. The intensity and the position of these new peaks appearing upon incorporation of second and third shell scattering atoms will depend on the position of the imidazole rings, but we do not explore this structural feature here. The three-shell calculation also lacks agreement with the spectra of the derivatives shown in Fig. 3 in the energy region of band *A*. This band is very weak (or possibly absent) in the experimental spectra. Therefore, a three-coordinate, three-shell C_{3v} model does not adequately simulate the spectra for the Hc derivatives.

We have also calculated spectra for a hypothetical model, $Co(Imid)_3O$, with an additional ligand atom bound in the first shell (i.e., $Co\text{-}N_3O\text{-}C_6\text{-}C_3N_3$). This pseudo-tetrahedral model has three imidazole nitrogens occupying three vertices at 1.95 Å and an oxygen ligand occupying the fourth coordination position at a distance of 1.8 Å on the *z* axis. We note here that nitrogen and oxygen atoms are practically indistinguishable in XANES spectra, as in EXAFS, because their backscattering amplitudes and phases are very similar (Teo and Lee, 1979). The single-shell calculation in both polarizations (not shown) were very similar to the calculated tetrahedral CoN_4 cluster shown in Fig. 2. The calculated three-shell polarized XANES spectra are shown at the bottom of Fig. 5. The most important effect due to introduction of a fourth ligand is the quenching of the *E//z* polarized *A* band. For this reason, the simulation for this four-coordinate model

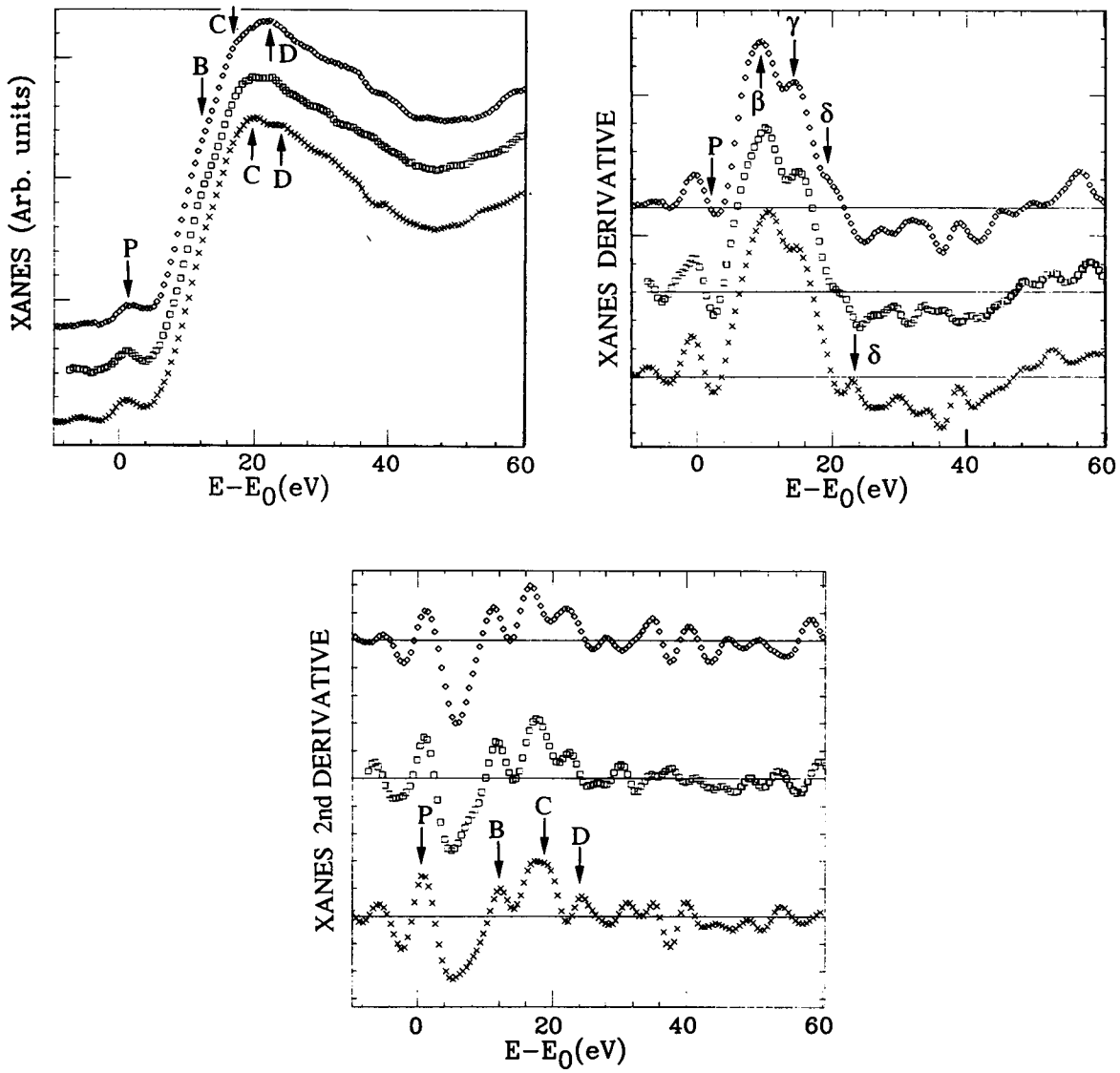

FIGURE 3 (*A*) Co K-edge XANES spectra for Co(II)-substituted *C. maenas* hemocyanin: dinuclear $Co(II)_2$-Hc derivative in sucrose solution (*bottom curve*); lyophilized dinuclear $Co(II)_2$-Hc derivative (*middle curve*); and lyophilized mononuclear Co(II)-Hc derivative (*top curve* (*B*) First derivative spectra in the same order as in *A*. (*C*) Second derivative spectra (multiplied by -1) in the same order as in *B*. The second derivative spectrum is useful to identify the energy position of the weak spectral features *B* and *C*.

fits the experimental data better than the three-coordinate model considered above (see below). The top of Fig. 5 shows the unpolarized spectrum of the tetrahedral-like model after application of broadening terms. The unpolarized calculation is used to compare the experimental and theoretical spectra more readily.

In Fig. 6 we superimpose this calculation on the XANES spectrum of the lyophilized dinuclear $Co(II)_2$-Hc, after alignment of the spectra obtained by subtracting 7 eV from the theoretical spectrum. The energies of the peaks are shown in Table 2. Although the correspondence between data and the calculated spectrum is good, there are discrepancies that have two contributing factors: 1) the expected disagreement between theoretical and experimental peak intensities, especially in the pre-edge peak; 2) the degree of distortion of the real atomic cluster from the symmetry of the model.

Fig. 7 shows a comparison of the first derivative of the calculated spectrum with those of the lyophilized dinuclear $Co(II)_2$-Hc (*bottom*) and the lyophilized mononuclear Co-(II)-Hc. The low-energy region of the theoretical spectrum (localized states) fits the data for both derivatives very well: therefore the distortion of the first shell from the symmetry of the model cluster is small. The calculated spectrum fits that of the dinuclear derivative better than the mononuclear derivative. Furthermore, the pre-edge peak intensity in the experimental spectrum for the binuclear derivative is more pronounced than for the mononuclear derivative. These observations suggest that the ligand geometry in the dinuclear derivative is closer to the tetrahedral case.

The results at this point in our analysis are consistent with a four-coordinate binding site for the Co(II) ions of both the mono- and dinuclear derivatives, based on similarities to the

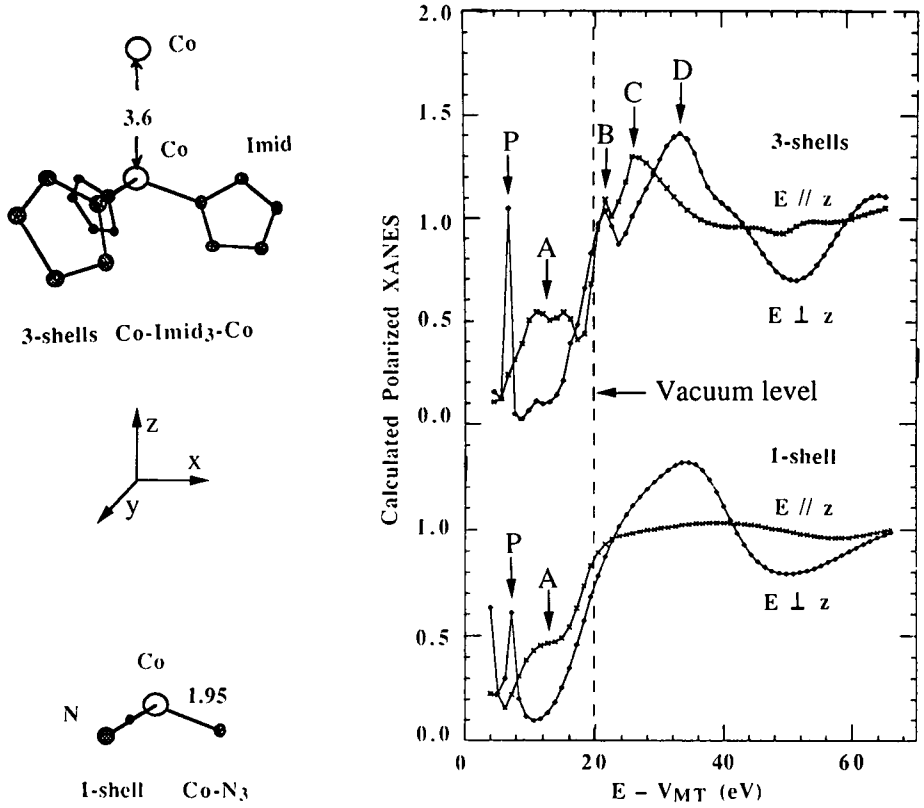

FIGURE 4 Calculated polarized Co K-edge XANES spectra of C_{3v} symmetry "deoxy-like" model: single-shell Co-N_3 cluster (*bottom*); three-shell Co(Imid)$_3$-Co cluster (*top*).

spectra of model complexes and on the simulations for the pseudo-tetrahedral cluster with four ligands. We considered extending our analysis to include hypothetical oxygenated cobalt sites since there is a report (Dutton et al., 1990) of oxygen binding to a dinuclear cobalt derivative of *L. polyphemus* Hc. Since the XANES spectra indicated the presence of Co(II), it seemed unlikely for there to be oxygen bound to the active site in the dinuclear derivative: oxygenated cobaltous complexes are formally cobaltic-superoxide or dicobaltic-peroxide (Michailidis and Martin, 1969; Morris and Martin, 1969). Spectra were nevertheless simulated for two five-coordinate models containing three imidazoles, plus a molecule of dioxygen (i.e., Co-N_3O_2-C_6-C_3N_3Co) (Fig. 8). The oxygen molecule in native Hc (Magnus and Ton-That, 1992) and in an oxygenated dinuclear Cu model compound (Kitajima et al., 1989) is bound as a μ:η^2-η^2 peroxo-dinuclear copper complex. In the first of these "oxy" models, the imidazole ring geometry is the same as in the deoxy-like configuration of Hc described above. In the second, the overall geometry is square pyramidal and the Co atom lies in a plane defined by two imidazole nitrogens and the oxygen atoms of the dioxygen molecule. The third imidazole nitrogen occupies the apical position. The bond lengths of the first shells in these models are all set to 1.95 Å (Feiters, 1990). Whether these models are relevant or not to the actual chemical species that would be present in an oxygenated site is superseded by the fact that they also serve to simulate spectra for higher coordination number Co(II) complexes not considered above.

The first derivatives of the calculated unpolarized spectra for the four active site models (going from three-coordinate deoxy- to five-coordinate oxy-) are shown in Fig. 8. Large differences are seen in the amplitude of the β and γ peaks. In the deoxy-like cluster (*bottom curve*), the high intensity of the peak β and the presence of the peak α originate from the *A* band (seen in Figs. 4 and 5). In the simulations of the oxygenated models, the increase of the β and γ peaks is a consequence of the increased coordination number of Co. Moreover, in the spectrum of the square pyramidal oxy-Co cluster (*top curve*), the feature corresponding to the pre-edge peak *P* is quenched. Consideration of these calculated spectra leads to the conclusion that only the four-coordinate model fits the experimental data well. Therefore, the simulations confirm that Co in the derivatives studied here is four-coordinate and has pseudo-tetrahedral geometry and rule out the possibility that the dinuclear derivative contains μ:η^2-η^2 bound dioxygen. Even if from the XANES simulations we cannot exclude the presence of dioxygen bound end-on in *cis-* or *trans-* mode to the two Co atoms (in this way each Co would be four-coordinated), the cobaltous oxidation state rules out the presence of an oxygenated site. Recent investigations on the temperature dependence of optical spectra of Co(II)-Hc (Vitrano et al., 1993), are consistent with the presence of an exogenous ligand strongly bound to the two metal ions of the dinuclear derivative. Independent structural data giving the Co-Co distance in the dinuclear and mononuclear derivatives could confirm this indication.

Cu(I)Co(II) *C. maenas* hemocyanin

Finally, we have investigated the structure of both the Co site and the Cu site in the hybrid Cu(I)-Co(II)-Hc derivative of

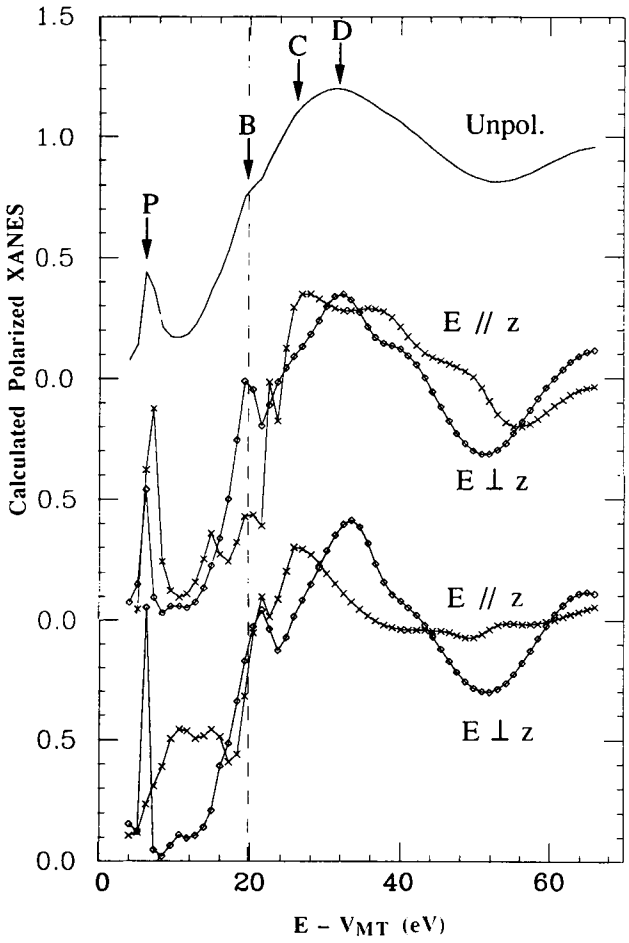

FIGURE 5 Calculated Co K-edge XANES spectra of three-shell "deoxy-like" three-coordinate model (*bottom curves*, as in Fig. 4) and pseudo-tetrahedral model: polarized spectra of the three-shell $Co(Imid)_3$-O cluster (*middle curves*); unpolarized spectrum of the same cluster (*top curve*) after the application of broadening terms (see Methods).

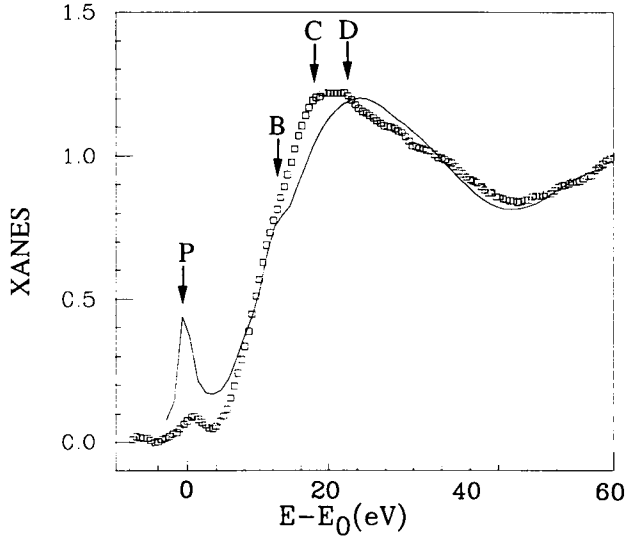

FIGURE 6 Calculated Co K-edge XANES unpolarized spectrum of the pseudo-tetrahedral model after the application of broadening terms (*solid line*); experimental XANES spectrum of the lyophilized dinuclear $Co(II)_2$-Hc derivative (*diamonds*). The spectra are aligned at the pre-edge peak *P*.

TABLE 2 Energy position of the features in CoK-edge spectra (± 0.5 eV)

		A	B	C	D	β	γ
Calcualted*	0.0	8.0	13.0	19.0	25.0	11.0	17.0
$Co(II)_2$-Hc‡	0.0		11.5	18.0	23.5	10.5	15.5

* Calculated value − 7 eV.
‡ Lyophilized sample.

C. maenas hemocyanin. This species was reported to contain one mole of Cu(I) and one mole of Co(II), based on atomic absorption and results of optical and EPR spectra (Bubacco et al., 1992). Fig. 9 shows the Co K-edge XANES spectra of lyophilized $Co(II)_2$-Hc (*bottom*) and that of the lyophilized hybrid (*top*). The spectrum of the hybrid Hc shows the same features, including the prominent pre-edge peak, *P*, at the same energies as the dinuclear $Co(II)_2$-Hc. Therefore, the hybrid metal active site also contains four-coordinate pseudo-tetrahedral Co(II).

In Fig. 10, we compare the Cu K-edge XANES spectra of the lyophilized hybrid Cu(I)Co(II)-Hc (*bottom spectrum*), with that of lyophilized oxy-Hc (*diamonds*) and deoxy-Hc (*circles*). It should be noted that the spectrum of the oxy-form arises from cupric copper and that of the deoxy- form from threefold coordinated cuprous copper in the active site (Brown et al., 1980). The spectrum of the hybrid Hc shows the prominent structured shoulder at 6–8 eV typical of three-coordinate Cu(I) (Kau et al., 1987). This result indicates that the copper in the hybrid has an electronic and geometric structure very similar to that in deoxy-Hc. Since both metals of the hybrid exhibit the spectra of their counterparts in the dinuclear sites, these results suggest they both occupy the active site. We note here that samples of the hybrid derivative may contain small amounts of oxy-Hc due to incomplete conversion with Co(II) (Bubacco et al., 1992), but no attempt was made to quantitate its contribution in the spectrum of this species.

The same structural feature indicated for the origin of the *A* band in the Co "deoxy-like" cluster shown in Fig. 4 contributes to the shoulder in the Cu K-edge of deoxy-Hc. From the one-electron formalism (Muller and Wilkins, 1984) it is known that the overall magnitude and shape of a particular spectrum is determined by the $n\ell \rightarrow \epsilon(\ell + 1)$ atomic transition probability which has a rather smooth energy dependence, and varies weakly with the atomic number *Z*. The fine structure of the spectrum is determined by a solid state factor proportional to the density of states with $\ell + 1$ orbital character, and therefore depends on the atomic environment. Extensive studies (Kutzler et al., 1980; Bianconi, 1988) on transition metal ions in tetrahedral complexes (such as $[MnO_4]^-$ in solution, $[CrO_4]^{2-}$ and $[VO_4]^{3-}$ in crystals), Ti and Fe in glass, and metal oxides (Norman et al., 1985) confirm that

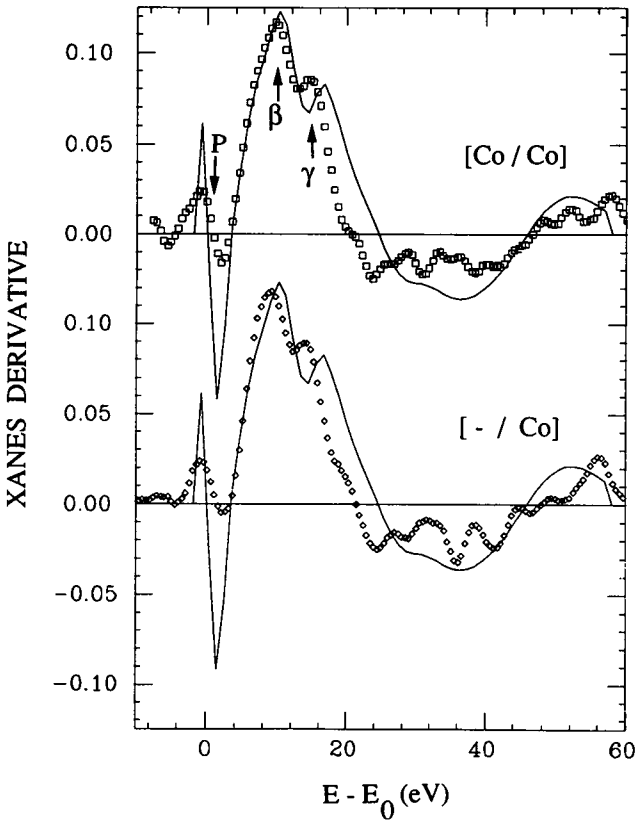

FIGURE 7 First derivative of the XANES spectrum of the pseudo-tetrahedral model (*solid line*) shown with the first derivative spectra of the lyophilized dinuclear $Co(II)_2$-Hc (*squares, top*) and the lyophilized mononuclear Co(II)-Hc (*diamonds, bottom*).

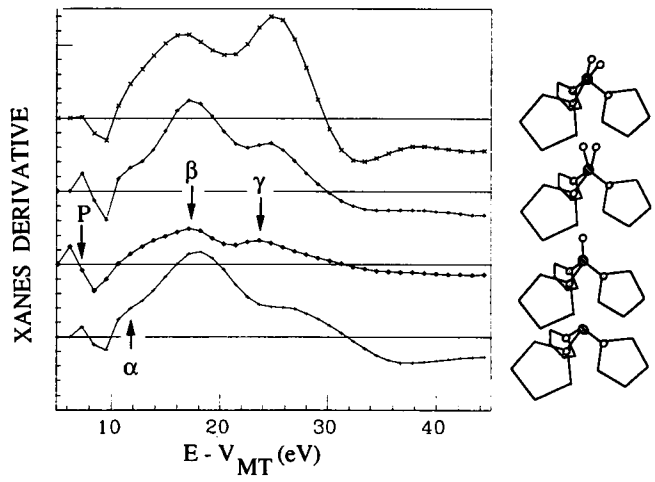

FIGURE 8 First derivative of calculated XANES spectra of model clusters. From *bottom* to *top:* 1) C_{3v} "deoxy-like" cluster with three-coordinate Co(II); 2) pseudo-tetrahedral cluster; 3) "oxy-like" model with five-coordinate Co(II) obtained by adding an oxygen molecule to the "deoxy-like" model; and 4) "oxy-like" model with a square pyramidal five-coordinate Co(II).

the shape of the continuum resonances of the K-XANES spectrum depends on the atomic environment, more than on the particular absorbing atom.

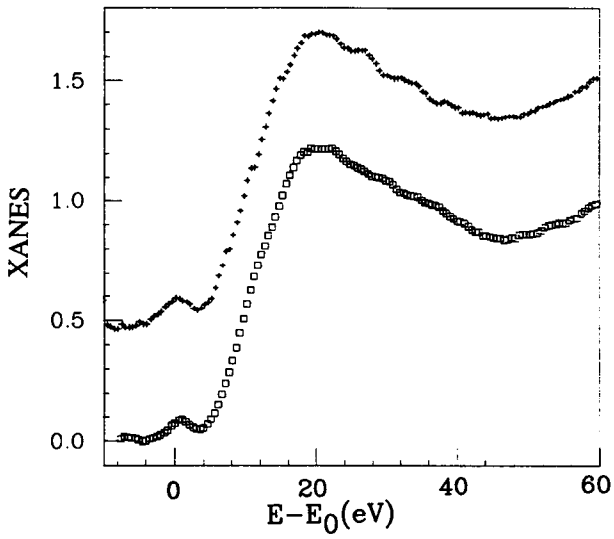

FIGURE 9 Co K-edge XANES spectra of lyophilized *C. maenas* Co-$(II)_2$-Hc (*bottom*) and (*top*) lyophilized *C. maenas* Cu(I)-Co(II)-Hc.

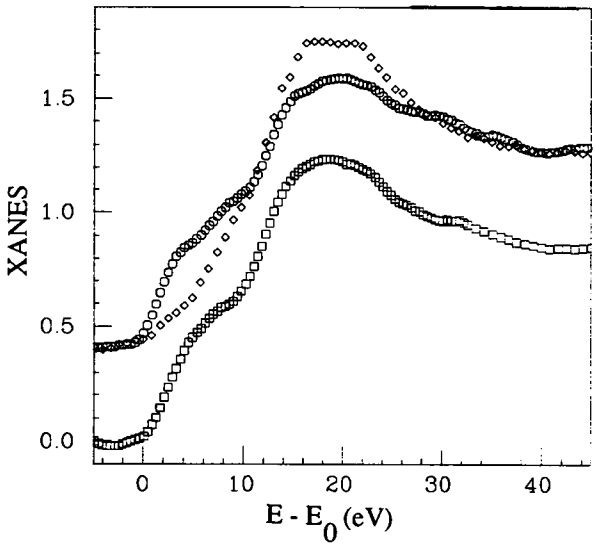

FIGURE 10 Cu K-edge XANES spectra of *C. maenas* Hc: *bottom,* lyophilized hybrid *C. maenas* Cu(I)Co(II)-Hc; *top,* lyophilized native oxy-Hc (*diamonds*) and deoxy-Hc (*circles*). The active site of oxy-Hc contains a dicupric-peroxide complex and the deoxy-Hc a dicuprous complex.

CONCLUSIONS

Earlier reports describe several cobalt-substituted Hc derivatives for which a distorted tetrahedral coordination geometry was inferred from optical spectroscopic properties alone, in spite of the presence of excess cobalt bound to the protein (Suzuki et al., 1982; Loroesch and Haase, 1986; Dutton et al., 1990). In the present report, a structural characterization was achieved for cobalt specifically bound to the active site. The analysis of XANES spectra of Co(II) derivatives of hemocyanin shows that the metal binding sites in mononuclear and dinuclear Co(II)-Hc is four-coordinate. This conclusion is based on similarities between the spectra of the Hc derivatives and those of model complexes and on the agreement

with simulated spectra using MS calculations. Furthermore, the geometry of the first shell is pseudo-tetrahedral, with three imidazole nitrogen ligands and a fourth ligand, possibly oxygen from a water ligand.

The first derivative spectra of mono and dinuclear Co(II)-Hcs show all features at the same energy, suggesting that the metal ligands and the first shell ligand bond lengths are the same for each metal ion bound. This result demonstrates structurally equivalent binding sites for both Co(II) ions in the dinuclear derivative and, therefore, is consistent with both ions being bound in the active site, known to be symmetrical from the crystallographic analysis of the copper-containing protein (Gaykema et al., 1984).

The spectrum of the dinuclear derivative is more closely related to the calculated XANES spectrum for an ideal tetrahedral case than that of the mononuclear derivative and shows an increased intensity of the 1s → 3d pre-edge peak. Therefore, the geometry of both Co(II) sites changes toward more tetrahedral when two Co(II) ions are loaded into the active site of the protein. These results are consistent with previously reported optical spectroscopic findings showing a larger optical extinction coefficient and a decreased ellipticity per Co(II) in the dinuclear derivative, as compared to the mononuclear derivative. These last findings were previously interpreted by assigning greater tetrahedral character to the metal bound in the dinuclear species (Bubacco et al., 1992).

Finally, Cu(I)-Co(II)-Hc contains four-coordinate pseudo-tetrahedral Co(II) and three-coordinate Cu(I) in the hybrid active site. Thus, the Co(II) in the hybrid is similar in geometry to the Co(II) in the dinuclear derivative while the Cu(I) is bound as in deoxy-Hc.

We acknowledge Prof. G. O. Morpurgo and Prof. C. Ercolani of Department of Chemistry, University "La Sapienza" of Rome, who kindly supplied the model compounds $Co(Et_4dien)Cl_2$ and CoL_2.

This work was supported by grants GM-40168 and RR-02583 from the National Institutes of Health, by grant INT 8714550 from the National Science Foundation, and by a grant from the GNCB-CNR, Italy.

REFERENCES

Amiconi, G., R. Santucci, M. Coletta, A. Congiu Castellano, A. Giovannelli, M. Dell'Ariccia, S. Della Longa, M. Barteri, E. Burattini, and A. Bianconi. 1989. Influence of globin structure on the heme in dromedary carbonmonoxyhemoglobin. *Biochemistry*. 28:8547–8553.

Bianconi, A. 1988. XANES spectroscopy. *In* X-ray Absorption: Principles, Applications, Techniques of EXAFS, SEXAFS, and XANES. D. C. Koningsberger and R. Prinz, editors. J. Wiley and Sons, New York. 573–662.

Bianconi, A., A. Congiu Castellano, P. J. Durham, S. S. Hasnain, and S. Phillips. 1985. The CO bond angle of carboxymyoglobin determined by angular-resolved XANES spectroscopy. *Nature (Lond.)*. 318:685–687.

Bianconi, A., J. Garcia, and M. Benfatto. 1988. XANES in condensed systems. *In* Topics in Current Chemistry. Vol. 145. E. Mandelnow, editor. Springer-Verlag, Berlin. 29–67.

Blackburn, N. J., R. W. Strange, J. Reedijk, A. Volbeda, A. Farooq, K. D. Karlin, and J. Zubieda. 1989. X-ray absorption edge spectroscopy of Cu(I) complexes. Coordination geometry of Cu(I) in the reduced forms of copper proteins and their derivative with carbon monoxide. *Inorg. Chem.* 28:1349–1357.

Bracci, M., C. Ercolani, B. Floris, M. Bassetti, A. Chiesi-Villa, and C. Guastini. 1990. Molecular and electronic structure of the complexes formed by the Schiff base N-(o-hydroxybenzylidene) ferroceneamine with Co(II), Ni(II), Cu(II) and Zn(II). *J. Chem. Soc. Dalton Trans.* 1357–1363.

Brown, J. M., L. Powers, B. Kincaid, J. A. Larrabee, and T. G. Spiro. 1980. Structural studies of the hemocyanin active site. 1. EXAFS analysis. *J. Am. Chem. Soc.* 102:4210–4216.

Bubacco, L., R. S. Magliozzo, M. Beltramini, B. Salvato, and J. Peisach. 1992. Preparation and spectroscopic characterization of a coupled binuclear center in Co(II)-substituted hemocyanin. *Biochemistry*. 31:9294–9303.

Ciampolini, M., and G. P. Speroni. 1966. Five-coordinated complexes of the transition elements from manganese to zinc with Bis(2-dimethylaminoethyl)methylamine. *Inorg. Chem.* 5:45–49.

Co, M. S., K. O. Hodgson, T. K. Eccles, and R. Lontie. 1981. Copper site of molluscan oxy-hemocyanins. Structural evidence from x-ray absorption spectroscopy. *J. Am. Chem. Soc.* 103:984–986.

Congiu Castellano, A., S. Della Longa, A. Bianconi, M. Barteri, E. Burattini, G. Amiconi, P. Ascenzi, M. Coletta, and R. Santucci. 1991. Influence of allosteric effectors on the heme conformation of dromedary ferrous nitrosylhemoglobin detected by XANES spectroscopy. *Biochim. Biophys. Acta*. 1080:7–13.

Della Longa, S., A. Bianconi, I. Ascone, A. Fontaine A. Congiu Castellano, and G. Borghini. 1992. Dynamics of CO recombination in sperm whale myoglobin by dispersive XANES. *In* Particle and Fields Series 49: Synchrotron Radiation and Dynamic Phenomena. A. Beswick, editor. American Institute of Physics, New York. 397–406.

Di Vaira, M., and L. Orioli. 1969. Crystal and molecular structure of dichlorobis (2-dimethylaminoethyl) methylaminecobalt (II). *Inorg. Chem.* 8:2729–2734.

Doniach, S., M. A. Berding, T. Smith, and K. O. Hodgson. 1984. Theory of x-ray absorption edge spectra. *In* EXAFS and Near Edge Structure III. K. O. Hodgson, B. Hedman, and J. Penner-Hahn, editors. Springer Verlag, Berlin. 33–37.

Dooley, D. M., R. A. Scott, J. Ellinghaus, E. I. Solomon, and H. B. Gray. 1978. Magnetic susceptibility studies of laccase and oxyhemocyanin. *Proc. Natl. Acad. Sci. USA*. 75:3019–3022.

Dori, Z., R. Eisenberg, and H. B. Gray. 1967. The crystal and molecular structure of the five-coordinated complex dichloro-1,1,7,7-tetraethyldiethylenetriaminecobalt(II). *Inorg. Chem.* 6:483–486.

Durham, P. J., 1988. Theory of XANES. *In* X-ray Absorption: Principles, Applications, Techniques of EXAFS, SEXAFS, XANES. R. Prinz and D. Koningsberger, editors. J. Wiley and Sons, New York. 53–84.

Durham, P. J., J. B. Pendry, and C. H. Hodges. 1982. Calculation of x-ray absorption near edge structure, XANES. *Comput. Phys. Commun.* 25: 193–205.

Dutton, T. J., T. F. Baumann, and J. A. Larrabee. 1990. Cobalt(II)-substituted *Limulus polyphemus* hemocyanin: cobalt equilibria, ligand binding and oxygenation chemistry. *Inorg. Chem.* 29:2272–2278.

Ellerton H. D., N. F. Ellerton, and H. A. Robinson. 1983. Hemocyanin—a current perspective. *Prog. Biophys. Mol. Biol.* 41:143–248.

Feiters, M. C. 1990. X-ray absorption spectroscopic studies of metal coordination in zinc and copper proteins. *Comm. Inorg. Chem.* 11:131–134.

Fink, J., N. Nucker, H. Romberg, and S. Nakai. 1989. Electronic structure of high T_c superconductors by valence and core electron excitations. *In* High T_c Superconductors: Electronic Structure. A. Bianconi and A. Marcelli, editors. Pergamon Press, Oxford. 293–312.

Gaykema, W. P. J., W. G. J. Hol, J. M. Vereijken, N. M. Soeter, H. J. Bak, and J. J. Beintema. 1984. 3.2 Å structure of the copper-containing, oxygen carrying protein *Panulirus interruptus* hemocyanin. *Nature (Lond.)*. 309: 23–29.

Hong, M. K., D. Braunstein, B. R. Cowen, et al. 1990. Conformational substates and motions in myoglobin. *Biophys. J.* 58:429–436.

Kasuga, K., and M. Tsutsui, 1980. Some new developments in the chemistry of metallophtalocyanines. *Coord. Chem. Rev.* 32:67–95.

Kau, L., D. J. Spira-Solomon, J. E. Penner-Hahn, K. O. Hodgson, and E. I. Solomon. 1987. X-ray absorption edge determination of the oxidation state and coordination number of copper: application to the type 3 site in *Rhus vernicifera* laccase and its reaction with oxygen. *J. Am. Chem. Soc.* 109:6433–6442.

Kitajima, N., K. Fujisawa, Y. Moro-oka, and K. Toriumi. 1989. μ:η^2-η^2-peroxo binuclear copper complex $[Cu(HB(3, 5\text{-}iPr_2pz)_3]_2$ (O_2). *J. Am.*

Chem. Soc. 111:8975–8976.

Kitamura, M., S. Muramatsu, and C. Sugiura, 1987. Multiple scattering studies for Cl K XANES of KCl, $SrCl_2$ and CsCl crystals. *Phys. Stat. Sol. (b).* 142:191–202.

Kosugi, N., T. Yokoyama, K. Asakura, and H. Kuroda. 1984. Polarized Cu K-edge XANES of square planar $CuCl_4^{2-}$ ion. Experimental and theoretical evidence for shake-down phenomena. *Chem. Phys.* 91:249–256.

Krause, M. O., and J. H. Oliver. 1979. Natural widths of atomic K and L levels, Kα x-ray lines and several KLL auger lines. *J. Phys. Chem. Ref. Data.* 8:329–338.

Kutzler, F. W., C. R. Natoli, D. K. Misemer, S. Doniach, and K. O. Hodgson, 1980. Use of one-electron theory for the interpretation of near edge structure in K-shell x-ray absorption spectra of transition metal complexes. *J. Chem. Phys.* 73:3274–3288.

Lever, A. B. P. 1984. Inorganic Electronic Spectroscopy. Elsevier, Amsterdam. 420 pp.

Li, C., M. Pompa, S. Della Longa, and A. Bianconi. 1991. Electronic structure of La_2CuO_4 joint analysis of O K and Cu K and L_3 edge x-ray absorption spectra. *Physica C.* 178:421–431.

Linzen, B., N. M. Soeter, A. F. Riggs, et al. 1985. The structure of arthropod hemocyanins. *Science.* 229:519–529.

Loroesch, J., and W. Haase. 1986. Cobalt(II)-hemocyanin: a model for the cuprous deoxy protein giving evidence for a bridging ligand in the active site. *Biochemistry.* 25:5850–5957.

Magnus, K., and Hoa Ton-That, 1992. The crystal structure of the oxygenated form of *Limulus polyphemus* subunit II hemocyanin. *J. Inorg. Biochem.* 47:20.

Michailidis, M. S., and R. B. Martin. 1969. Oxygenation and oxidation of cobalt (II) chelates of amines, amino acids and dipeptides. *J. Am. Chem. Soc.* 91:4683–4689.

Morris, P. J., and R. B. Martin. 1969. Tetrahedral complexes of cobalt (II) with L-histidine, histamine, imidazole and *N*-acetyl-L-histidine. *J. Am. Chem. Soc.* 92:1543–1546.

Moser, F. H., and A. L. Thomas. 1983. The Phtalocyanines. Vols. 1 and 2. CRC Press, Boca Raton, FL. 473 pp.

Muller, J. E., and J. W. Wilkins. 1984. Band-structure approach to the x-ray spectra of metals. *Phys. Rev. B*29:4331–4348.

Norman, D., K. B. Garg, and P. J. Durham. 1985. The x-ray absorption near edge structure of transition metal oxides: a one-electron interpretation. *Sol. State Commun.* 56:895–898.

Palladino, L., S. Della Longa, A. Reale, M. Belli, A. Scafati, G. Onori, and A. Santucci. 1993. XANES of Cu(II)-ATP and related compounds in solution: quantitative determination of the distortion of the Cu site. *J. Chem. Phys.* 98:2720–2726.

Pendry, J. B. 1974. Low Energy Electron Diffraction. Academic Press, New York. 31–70.

Salvato, B., and M. Beltramini. 1990. Hemocyanin: molecular architecture, structure and reactivity of the binuclear copper active site. *Life Chem. Rep.* 8:1–47.

Salvato, B., M. Beltramini, A. Piazzesi, M. Alviggi, F. Ricchelli, R. S. Magliozzo, and J. Peisach. 1986. Preparation, spectroscopic characterization and anion binding studies of a mononuclear Co(II) derivative of *Carcinus maenas* hemocyanin. *Inorg. Chim. Acta* 125:55–62.

Sano, M., S. Komorita, H. Yamatera. 1992. XANES spectra of copper (II) complexes: correlation of the intensity of the 1s→3d transition and the shape of the complex. *Inorg. Chem.* 31:459–463.

Slater J. C. 1979. The Self-Consistent Field for Molecules and Solids; Quantum Theory of Molecules and Solids. McGraw-Hill, New York. 583 pp.

Solomon, E. I., D. M. Dooley, R. H. Wang, H. B. Gray, M. Cerdonio, F. Mogno, and G. L. Romani. 1976. Susceptibility studies of laccase and oxyhemocyanin using an ultrasensitive magnetometer: antiferromagnetic behavior of the type 3 copper in *Rhus* laccase. *J. Am. Chem. Soc.* 98: 1029–1031.

Suzuki, S., J. Kino, M. Kimura, W. Mori, and A. Nakahara. 1982. Structure of the active site of hemocyanin. Cobalt (II)-substituted squid hemocyanin. *Inorg. Chim. Acta* 66:41–47.

Teo, B. K., and P. A. Lee. 1979. Ab initio calculation of amplitude and phase function for extended x-ray absorption fine structure spectroscopy. *J. Am. Chem. Soc.* 101:2815–2832.

Vitrano E., A. Cupane, M. Leone, V. Militello, L. Cordone, B. Salvato, M. Beltramini, L. Bubacco, and G. P. Rocco. 1993. Low temperature optical spectroscopy of cobalt-substituted hemocyanin from Carcinus maenas. *Eur. Biophys. J.* 22:157–167.

Volbeda, A., and W. G. J. Hol. 1986. Three-dimensional structure of haemocyanin from spiny lobster *Panulirus interruptus*, at 3.2 Å resolution. *In* Invertebrate Oxygen Carriers. B. Linzen, editor. Springer Verlag, Berlin. 135–147.

Volbeda, A., and W. G. J. Hol. 1989. Crystal structure of Hexameric haemocyanin from *Panulirus interruptus* refined at 3.2 Å resolution. *J. Mol. Biol.* 209:249–279.

Woolery, G. L., L. Powers, M. Winkler, E. I. Solomon, and T. G. Spiro. 1984. EXAFS studies of binuclear copper site of oxy-, deoxy-, metaquo-, metfluoro-, and metazidohemocyanin from arthropods and molluscs. *J. Am. Chem. Soc.* 106:86–92.

Wyckoff, R. W. G., 1964. Crystal structures. Vol. 1. J. Wiley and Sons, New York. 270–272.

Yachandra, V., L. Powers, and T. G. Spiro. 1983. X-ray absorption spectra and the coordination number of Zn and Co carbonic anhydrase as a function of pH and inhibitor binding. *J. Am. Chem. Soc.* 105:6596–6604.